

Firing statistics of a neuron model driven by long-range correlated noise

J. W. Middleton,* M. J. Chacron, B. Lindner, and A. Longtin

Department of Physics, University of Ottawa, 150 Louis Pasteur, Ottawa, Ontario, Canada K1N 6N5

(Received 12 February 2003; published 28 August 2003)

We study the statistics of the firing patterns of a perfect integrate and fire neuron model driven by additive long-range correlated Ornstein-Uhlenbeck noise. Using a quasistatic weak noise approximation we obtain expressions for the interspike interval (ISI) probability density, the power spectral density, and the spike count Fano factor. We find unimodal, long-tailed ISI densities, Lorentzian power spectra at low frequencies, and a minimum in the Fano factor as a function of counting time. The implications of these results for signal detection are discussed.

DOI: 10.1103/PhysRevE.68.021920

PACS number(s): 87.17.Aa

I. INTRODUCTION

Long-range correlations are ubiquitous in nature [1]. For example, it is known that natural images [2] as well as music [3] display long-range correlations. These signals serve as natural stimuli to neurons in the visual and auditory systems, respectively. It is known that these neurons exhibit long-range correlations in their spike trains [4,5], and there is much speculation as to the functional role these correlations might serve. For example, it has been proposed that long-range correlations in neurons provide some advantages in terms of matching the detection system to the expected signal [5,6].

The regularity shown by neural spike trains will have consequences on stimulus encoding and detection. It has been recently shown that both auditory neurons [5] and electroreceptors of weakly electric fish display both short-range anticorrelations and long-range correlations in the interspike interval (ISI) sequence [7,8]. Long-range correlations of different kinds, namely, long-range anticorrelation, have also been observed in paddlefish electroreceptors [9].

It has been shown that short-range anticorrelation and long-range correlation could contribute to give a minimum in spike train variability as measured by the Fano factor (variance-to-mean ratio of the spike count) at a behaviorally relevant time scale [8]. In that study the minimum was numerically observed for a leaky integrate-and-fire neuron with dynamic threshold (LIFDT) driven by periodic forcing and weak long-range correlated noise. Our study focuses on the sufficient conditions under which such a minimum can be obtained in a neuron model. Our results show that dynamic threshold, leakage, and periodic forcing are not necessary to obtain a nonmonotonous Fano factor. A perfect integrate-and-fire model driven by long-range correlated noise contains all the essential elements to reproduce a minimum in the Fano factor.

We also examine how the long-range correlated noise affects ISI statistics and the spike train power spectrum. The ISI densities and correlation measures are difficult to obtain analytically for the LIFDT, but are possible, with certain approximations, for the perfect integrate-and-fire neuron. Uni-

modal ISI densities with long tails are analytically obtained, and the correlation present in the driving noise source is shown to carry over to the ISI correlation coefficients. The structure of the power spectrum follows, as a consequence of the Fano factor shape. Analytic results are compared with results of numerical simulations throughout.

Section I presents the model system and outlines the approximations used for the analytics as well as the parameter regime under which they are valid. Section II characterizes the ISI statistics and shows how their properties reflect the properties of the input to the neuron. In Secs. III and IV the statistics of the output spike trains are analyzed by using the Fano factor, the spike-spike autocorrelation function, and the power spectral density. The analytic expression for the Fano factor agrees with the simulation results, revealing a minimum for this simple integrate-and-fire model. The implications of these results are finally discussed.

A. Model

Here we look at a simple neuron model, the perfect integrate-and-fire neuron, driven by Ornstein-Uhlenbeck (OU) noise, $\eta(t)$. The dynamical equations describing our system are

$$\begin{aligned}\frac{dv(t)}{dt} &= \mu + \eta(t), \\ \frac{d\eta(t)}{dt} &= -\frac{\eta(t)}{\tau} + \sqrt{\frac{2D}{\tau}}\xi(t),\end{aligned}\quad (1)$$

where $v(t)$ is the membrane voltage, μ is a constant bias, τ and D are, respectively, the correlation time and variance of the OU process, and $\xi(t)$ is Gaussian white noise with autocorrelation $\langle \xi(t)\xi(t') \rangle = \delta(t-t')$. The driving OU process has a Gaussian stationary probability density $\rho(\eta) = \exp[-\eta^2/2D]/\sqrt{2\pi D}$ and an exponential correlation function $\langle \eta(t)\eta(t') \rangle = D \exp[-|t-t'|/\tau]$. The voltage is reset to 0 once it reaches a threshold value v_{th} , without resetting $\eta(t)$. For all numerical results, unless stated otherwise we use the parameter values $v_{th} = 2\pi$ and $\mu = 1$. The times at which the voltage crosses threshold, $\{t_k\}$, will be the spike times of the resulting spike train given by the expression

*Email address: jmidd620@science.uottawa.ca

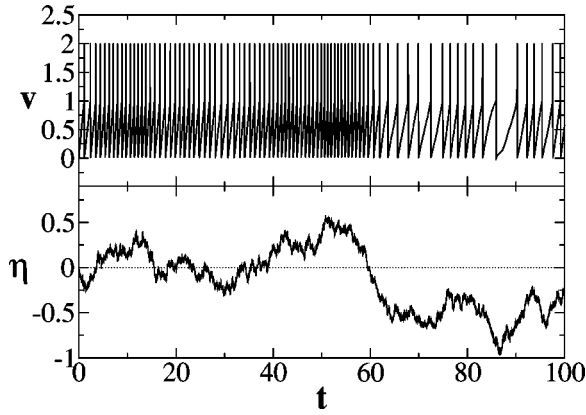


FIG. 1. A sample spike train with subthreshold voltage variations and the corresponding driving noise. The variance of the noise was set to a large value, $D=1$, which is used here to visually discern the modulation of the interspike intervals. The time constant used was $\tau=100$. The vertical bars on top of the voltage trace in the upper panel is not from the dynamics in Eq. (1), but were added to illustrate spikes.

$$x(t) = \sum_k \delta(t - t_k). \quad (2)$$

The spike count $N(t)$ [i.e., the number of spikes observed in a counting window $(0, t)$] is given by

$$N(t) = \int_0^t dt x(t) = \sum_{0 \leq t_k} \Theta(t - t_k), \quad (3)$$

where $\Theta(t)$ is the Heaviside step function. Figure 1 shows a realization of the membrane voltage $v(t)$ and its corresponding driving noise $\eta(t)$. This illustrates the slow modulating effects of the noise on the ISIs.

An equivalent spike train can be generated without the explicit reset of the voltage, but, instead, by incrementing the threshold by v_{th} every time the voltage reaches it. Spikes are generated each time the threshold is incremented. In this picture, without explicit voltage reset, the spike count at time t is equal to the threshold divided by the constant v_{th} . The freely evolving dynamics in Eq. (1) is equivalent to the Brownian motion of a particle on an inclined plane. Variables $v(t)$ and $\mu + \eta(t)$ are then viewed as the particle's position and velocity, respectively. Provided we have a finite positive bias, $\mu > 0$, the average difference between $v_{th}(N(t)+1)$ and $v(t)$ does not grow unbounded in time, whereas the standard deviation of $v(t)$ grows as \sqrt{t} , asymptotically. Consequently, in the asymptotic limit, the statistics of the threshold and of the counting process $N(t)$ become indistinguishable from the statistics of $v(t)$, as seen in Fig. 2.

B. Quasistatic approximation

We wish to look at the effect of long-range correlated noise, so we use a quasistatic approximation for the noise. If τ is much larger than the average ISI, then on short time scales η is approximately constant. In this way we can relate each ISI to a unique value of the OU process

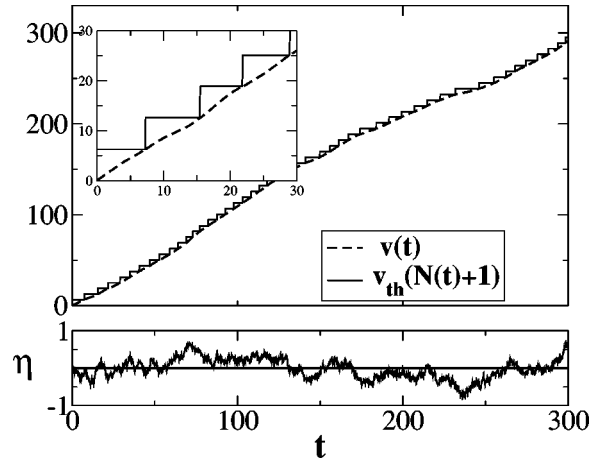


FIG. 2. The freely evolving voltage $v(t)$ and the increment threshold variable (upper panel) driven by the OU process $\eta(t)$ (lower panel). The difference between the threshold variable and the voltage is only noticeable on smaller scales (inset).

$$I_k = \frac{v_{th}}{\mu + \eta_k}, \quad (4)$$

where k denotes the index in a sequence of ISIs, and η_k is the value of η at the beginning of the k th interval. Equation (4) is a good approximation as long as $\eta_k > -\mu$ and $I_k \ll \tau$. As η_k approaches $-\mu$ from above, the ISI obtained from the static-noise approximation diverges and is negative for $\eta_k < -\mu$. This is problematic as negative ISIs have no physical meaning. In order to minimize the occurrence of these values we require that

$$D = \langle \eta^2 \rangle \ll \mu^2, \quad (5)$$

i.e., we use weak long-range correlated noise. Whenever the noise attains values close to or below $-\mu$, the ISI will be of the order of magnitude of the correlation time τ , during which the OU process returns to values greater than $-\mu$. Clearly, those ISI realizations are not captured by Eq. (4); however, their occurrence will be rare due to Eq. (5) and thus their influence on the firing statistics is negligible.

Approximation (4) not only allows us to write down a conditional probability density function (PDF) between I_k and η_k , but also allows us to reduce this conditional PDF to a δ function due to the unique one-to-one correspondence between η_k and I_k :

$$P(I_k | \eta_k) = \delta\left(I_k - \frac{v_{th}}{\mu + \eta_k}\right). \quad (6)$$

II. INTERSPIKE INTERVAL STATISTICS

A. Stationary probability density function

The first quantity of interest is the stationary PDF of ISIs. In order to obtain the stationary ISI PDF we can average the conditional PDF between I_k and η_k over all values of η_k :

$$P(I_k) = \int_{-\infty}^{\infty} d\eta_k P(I_k | \eta_k) \rho(\eta_k). \quad (7)$$

The statistics of the values of the OU process sampled at the beginning of each ISI, η_k , are not the same as for the continuous OU process, η . Imagine we measure the noise value at the beginning of each interspike interval of a long spike train. Then a higher value of noise leads to a shorter interval and hence to more intervals within a given time period than a lower value of η . This problem is known as biased sampling of a stochastic variable [10] and is resolved by a corrective factor given by the inverse interspike interval (see also Ref. [11]). Normalization of the corrected PDF yields

$$\rho(\eta_k) = \frac{e^{-\eta_k^2/2D}}{\sqrt{2\pi D}} \left(1 + \frac{\eta_k}{\mu}\right). \quad (8)$$

For simplicity, this normalization as well as any integration in the remainder of the paper is performed with respect to the full range of noise values, including $\eta < -\mu$, since these values will make a negligible contribution to the integrals we perform. Inserting Eq. (8) into Eq. (7) yields the PDF for the interspike interval density:

$$\begin{aligned} P(I_k) &= \int_{-\infty}^{\infty} d\eta_k \delta\left(I_k - \frac{v_{th}}{\mu + \eta_k}\right) \frac{e^{-\eta_k^2/2D}}{\sqrt{2\pi D}} \left(1 + \frac{\eta_k}{\mu}\right) \\ &= \int_{-\infty}^{\infty} d\eta_k \delta\left(\eta_k - \frac{v_{th}}{I_k} + \mu\right) \frac{e^{-\eta_k^2/2D}}{\sqrt{2\pi D} v_{th} \mu} (\mu + \eta_k)^3 \\ &= \frac{v_{th}^2}{\sqrt{2\pi D} \mu} \frac{\exp[-(\mu I_k - v_{th})^2 / (2D I_k^2)]}{I_k^3}. \end{aligned} \quad (9)$$

Using these densities the means for the sampled stationary OU process and ISI are, respectively, D/μ and v_{th}/μ . Note, however, that the PDF decays as $1/I_k^3$ for large I_k according to a power law, in contrast to the white noise driven case [12]. This implies a divergence for the second and higher moments revealing again that the approximation made is restricted to ISIs smaller than τ .

Figure 3(a) shows the stationary PDF for fixed τ and several values of D from both numerical simulation of Eq. (1) and the corresponding theoretical curves using Eq. (9). With increasing noise the mean of the density does, in fact, remain the same at v_{th}/μ , because the shift of the peak towards smaller ISI values is balanced out by the long tails for larger ISI values. Even though we began with a weak noise condition (5), the theoretical densities agree with simulation results very well beyond this condition. The agreement holds even for higher noise values (i.e., $D = 1$), though not as well for smaller noise values.

Figure 4 shows the simulation and theoretical PDFs for fixed D and various values of τ . The numerical results agree well with the theory, but the agreement breaks down when τ is on the order of the mean ISI. For shorter values of τ , i.e., $\tau < v_{th}/\mu$, the quasistatic approximation is no longer valid.

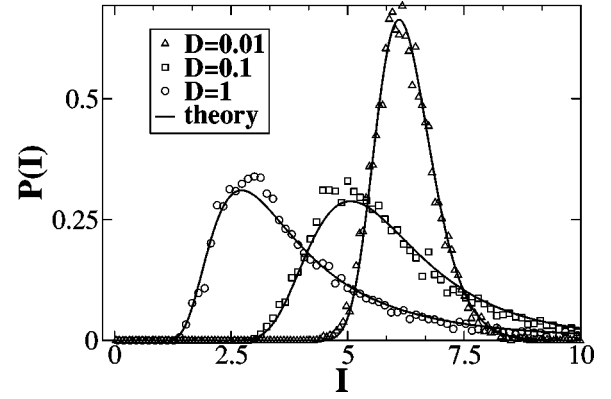


FIG. 3. Stationary ISI probability densities. Numerical simulations for fixed $\tau = 1000$ and different values of variance D along with the theoretical probability densities (9). Note that the mean is v_{th}/μ in all cases.

B. Serial correlation coefficient

The serial correlation coefficient (SCC) is a measure of correlation between different elements in a sequence of random events. The SCC, ρ_l in this case, is between two ISIs separated by l intermediate ones. The number l is referred to as the lag, and the SCC at lag l is given by

$$\rho_l = \frac{\langle I_k I_{k+l} \rangle - \langle I_k \rangle \langle I_{k+l} \rangle}{\langle I_k^2 \rangle - \langle I_k \rangle^2}, \quad (10)$$

where the averages here are over an ensemble of ISI sequences. The mean values for the k th and the $(k+l)$ th ISIs are the same if the process giving rise to these ISIs is stationary. A simple expression for these SCCs can be obtained first by taking the Taylor expansion of Eq. (4) about $\eta_k = 0$:

$$I_k \approx \frac{v_{th}}{\mu} \left(1 - \frac{\eta_k}{\mu}\right), \quad (11)$$

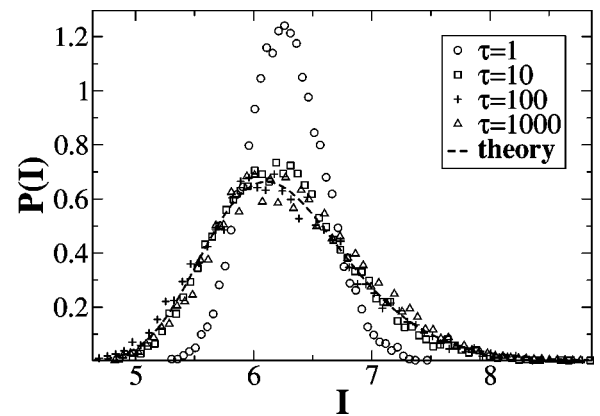


FIG. 4. Stationary ISI probability densities. Numerical simulations for $D = 0.01$ and different values of the correlation time τ . The theoretical result (9) is independent of τ because of the quasistatic approximation. The quasistatic approximation is not valid for small values of τ .

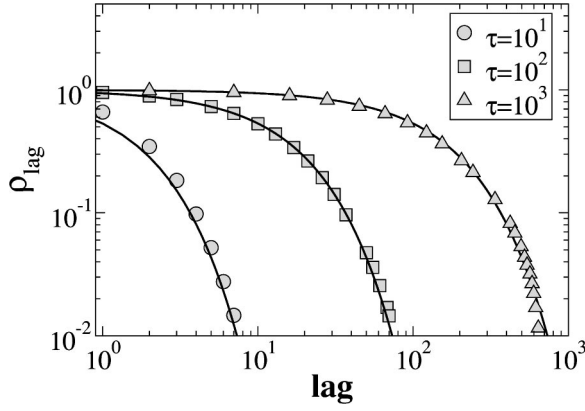


FIG. 5. The serial correlation coefficient from numerical simulation (symbols) and theoretical result (13) (solid lines). Results for three values of the noise correlation time are shown. The variance of the noise used in simulations is $D=0.01$; the theoretical curves are independent of the driving noise strength.

provided assumption (5) still holds. We may then approximate the serial correlation coefficient by inserting Eq. (11) into Eq. (10):

$$\rho_l \approx \frac{\langle \eta_k \eta_{k+l} \rangle - \langle \eta_k \rangle^2}{\langle \eta_k^2 \rangle - \langle \eta_k \rangle^2} \equiv C_{\eta_k}(l), \quad (12)$$

which is simply the autocorrelation function of the sampled OU process. For low noise, the times t_{k+l} at which the process is sampled do not deviate much from $t_k + l\langle I \rangle$. This allows us to estimate the ISI correlation:

$$\begin{aligned} \rho_l &\approx C_{\eta_k}(l) \approx C_{\eta}(l\langle I \rangle) \\ &= \exp\left[-\frac{lv_{th}}{\mu\tau}\right] = \exp\left[-\frac{l\langle I \rangle}{\tau}\right]. \end{aligned} \quad (13)$$

Although this formula is just a simple estimate, it fits the simulation data, Fig. 5, rather well. Deviations become apparent for moderate values of the correlation time τ (i.e., in Fig. 5, $\tau=10\approx\langle I \rangle$) and for larger values of the noise variance (not shown). Numerical simulations have shown that for extremely large correlation times the noise variance needs to be scaled down appropriately in order to maintain agreement with the theoretical expression, Eq. (13). Details will be given elsewhere. Apart from these small deviations, we can state that for weak long-range correlated noise, the exponential correlation of the noise carries over to the ISI statistics and that the “correlation lag” (i.e., the discrete counterpart of a correlation time) is given by

$$l_{\text{corr}} = \frac{\tau}{\langle I \rangle} = \frac{\tau\mu}{v_{th}}. \quad (14)$$

III. FANO FACTOR

A. Large-time analytic approximation

The Fano factor [13] $F(t)$ is the variance to mean ratio of a counting process $N(t)$ for a given counting time t . It is

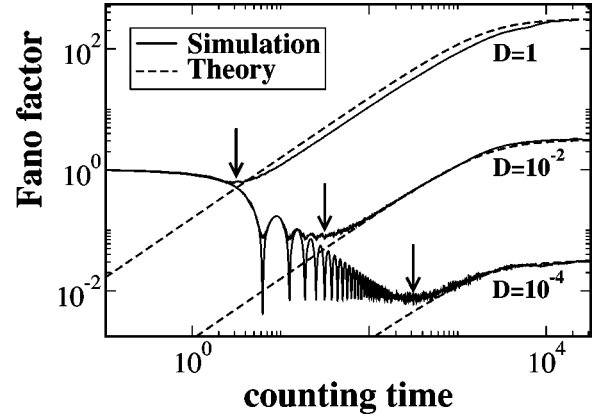


FIG. 6. The numerical results (solid lines) of the Fano factor for different noise intensities with $\tau=1000$ for the system of Eq. (1). The dashed lines are the theoretical curves obtained from Eq. (15). This theory is valid only in the large counting time limit. The arrows indicate the positions of the minimum in the Fano factor as given by Eq. (23).

useful for determining on which time scales the process is most regular. As discussed in the Introduction, the spike count process is equivalent to the freely evolving dynamics of a particle executing Brownian motion on an incline in the asymptotic time limit. In this limit we can use the statistics of the two processes interchangeably, so that we can use the well-known Fano factor for Brownian motion [14] as an approximation for the Fano factor of the spike count for large times:

$$F_{\text{large}}(t) = \frac{2D\tau}{v_{th}\mu} \left[1 - \frac{\tau}{t} (1 - e^{-t/\tau}) \right]. \quad (15)$$

It is readily seen that for moderate time, $t < \tau$, the Fano factor is $F_{\text{large}} \approx Dt$ (no τ dependence), whereas for $t \rightarrow \infty$ we have $F_{\text{large}} \approx D\tau$ (i.e., saturation). Hence, the linear growth of the Fano factor in time (corresponding to the ballistic phase of Brownian motion) is determined only by the variance of noise values, while the correlation sets where the ballistic phase terminates. Figure 6 shows $F_{\text{large}}(t)$ for different variances of the OU process with $\tau=10^3$. Theoretical curves (15) converge toward the numerical results for a sufficiently long counting time. The convergence is faster for intermediate noise values, as seen in Fig. 6. The Fano factor curves reach an asymptotic value, given by

$$\lim_{t \rightarrow \infty} F_{\text{large}}(t) = \lim_{t \rightarrow \infty} F(t) = \frac{2D\tau}{v_{th}\mu}. \quad (16)$$

B. Short-time analytic approximation

The Fano factor of the random point process described by our neuron with long-range noise (1) approaches 1 in the limit $t \rightarrow 0$, which is the Poissonian limit [10]. Equation (15) is only valid in the large time limit and fails to capture the discrete nature of the point process, which becomes apparent at small times (see Fig. 6). If an approximation of the Fano factor for short counting window times can be found, we

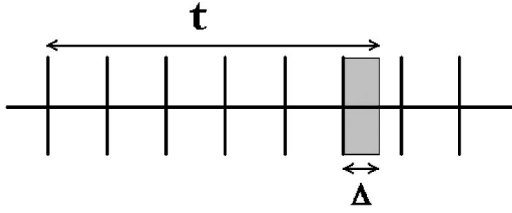


FIG. 7. A regularly spaced spike train. Δ is the fraction of an ISI that remains after taking out the largest number of ISIs from the counting time t .

can use this expression as well as the large time approximation (15) to interpolate values of the Fano factor at intermediate time scales.

The intensity of the long-range correlated noise is small in our approximation. Consequently, over short counting times the spike train appears very regular. Because of this regularity the Fano factor for a deterministic spike train will be a good approximation. Figure 7 shows such a spike train with a given counting time t . The variable Δ [used here as shorthand for $\text{mod}(t, \langle I \rangle)$] is the difference in time between t and the largest number of integer multiples of $\langle I \rangle$ that t contains. We shall refer to this largest integer as k , which gives us $t = k\langle I \rangle + \Delta$. As Fig. 7 shows, for a given t , the spike count N can take on only one of the two values: k or $k+1$. The probabilities of observing these counts are

$$P(i) = \begin{cases} 1 - \frac{\Delta}{\langle I \rangle}, & i = k \\ \frac{\Delta}{\langle I \rangle}, & i = k+1 \\ 0, & \text{otherwise,} \end{cases} \quad (17)$$

where i is the index of the spike in the deterministic spike train. From $P(i)$ we can obtain the mean and variance of the spike count:

$$\langle n \rangle = \frac{t}{\langle I \rangle} \quad (18)$$

and

$$\langle n^2 \rangle = \sum_{i=0}^{\infty} i^2 P(i) = k^2 + 2k \frac{\Delta}{\langle I \rangle} + \frac{\Delta}{\langle I \rangle} \quad (19)$$

and thus the variance becomes

$$\langle n^2 \rangle - \langle n \rangle^2 = \frac{\Delta}{\langle I \rangle} \left(1 - \frac{\Delta}{\langle I \rangle} \right). \quad (20)$$

From this, we can obtain an expression for the Fano factor for small counting times:

$$F_{\text{small}}(t) = \frac{\langle n^2 \rangle - \langle n \rangle^2}{\langle n \rangle} = \frac{\Delta}{t} \left(1 - \frac{\Delta}{\langle I \rangle} \right). \quad (21)$$

The variance of the deterministic regular spike train is a periodic sequence of inverted parabolas with a local maximum

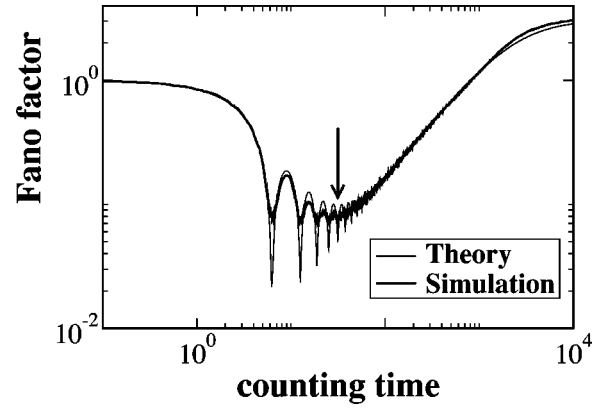


FIG. 8. Comparison of the numerically obtained Fano factor along with the complete short- and long-time theoretical Fano factor from Eqs. (15) and (21) for $D=10^{-2}$ and $\tau=1000$. The arrow indicates the position of the minimum in the Fano factor, as given by Eq. (23). The numerical data is the same as in Fig. 6.

of $1/4$ located at every odd multiple of $\langle I \rangle/2$. Because the variance does not grow past a finite value in time, the Fano factor is damped out by the linearly increasing mean and becomes negligible at large time scales.

C. Full-range approximation

The sum of the short-time and the long-time approximations, $F(t) = F_{\text{small}}(t) + F_{\text{large}}(t)$, provides a good fit to data from numerical simulations over the full range of counting windows, as can be seen in Fig. 8. Figure 6 shows that for a finite range of noise intensities the Fano factor exhibits a minimum, and it is noteworthy that this crude approximation, $F_{\text{small}}(t) + F_{\text{large}}(t)$, gives a very good estimate for the position of the minimum in the Fano factor. By minimum we mean the first local minimum encountered in going from large time values to small ones. It was previously shown that a minimum in the Fano factor indicates an optimal time scale on which to detect two distinct signals [8,15]. Since the variance of the deterministic spike train, Eq. (20), is confined to the interval $[0, 1/4]$, the small time Fano curve can be approximated by the envelope of its oscillations, $F_{\text{small}} \approx \langle I \rangle/4t = v_{th}/4\mu t$. This agrees with our previous definition of the minimum of the Fano factor. This envelope and the large time Fano factor can be used to determine a minimum, given by

$$\frac{d}{dt} \left[\frac{v_{th}}{4\mu t} + \frac{2D\tau}{v_{th}\mu} \left(1 - \frac{\tau}{t} (1 - e^{-t/\tau}) \right) \right] = 0. \quad (22)$$

Since the position of the minimum is, in general, much smaller than τ , we can expand the exponential in Eq. (22) to second order and differentiate. Solving the resulting equation yields the approximate position of the minimum of the Fano factor:

$$t_{\min} \approx \frac{v_{th}}{2\sqrt{D}}. \quad (23)$$

Because we consider large correlation times τ , the times at which the sum of $F_{\text{small}}(t)$ and $F_{\text{large}}(t)$ gives a minimum occur only in the ballistic region of Brownian motion. Here, neither $F_{\text{small}}(t)$ nor $F_{\text{large}}(t)$ depend on τ . Hence, the minimum is determined by the only remaining parameter, namely the noise variance.

The positions of the minimum, as given by Eq. (23), are indicated by arrows in Figs. 6 and 8, which agree very well with the apparent positions of the minimum given by the numerical simulations. We have thus shown that Eq. (1) exhibits a minimum in the Fano factor, and that the position of this minimum does not depend on the correlation time τ in this quasistatic approximation, but is entirely determined by the variance of the noise.

IV. SPIKE TRAIN POWER SPECTRUM

We now derive correlation and spectral properties of the spike train generated by Eq. (1). The relation between the Fano factor and the spike autocorrelation function is given by [10]

$$F(t) = 1 + \frac{2}{f} \int_0^t ds \left(1 - \frac{s}{t} \right) R_{xx}^+(s), \quad (24)$$

where $f = \mu/v_{th}$ is the mean firing rate of the point process and $R_{xx}^+(t)$ is the autocorrelation function of the spike train for $t > 0$ (not including the δ function at the origin). We can invert this relation to find R_{xx}^+ in terms of the Fano factor

$$R_{xx}^+(t) = \frac{\mu}{2v_{th}t} \frac{d}{dt} \left(t^2 \frac{d}{dt} F(t) \right). \quad (25)$$

The power spectrum can be calculated by the Fourier transform of the autocorrelation function

$$S(f) = \int_{-\infty}^{\infty} dt e^{i2\pi ft} R_{xx}(t). \quad (26)$$

Due to the linearity of the differential operator acting on the Fano factor in Eq. (25), the correlation can be expressed as a sum of two contributions: one coming from the small time approximation of the Fano factor and the other from the large time approximation. The discontinuities in the derivatives of the small time approximation make the integration of its corresponding correlation function analytically difficult. If we limit our focus to the correlation function at large times (coming from the large time Fano factor), we can describe the power spectrum at low frequencies. Substituting the expression for the large-time Fano factor, Eq. (15), will give us the autocorrelation function for large times:

$$R_{xx}^+(t) = \frac{D}{v_{th}^2} e^{-t/\tau}. \quad (27)$$

Inserting this expression into Eq. (26) gives us a Lorentzian spectrum:

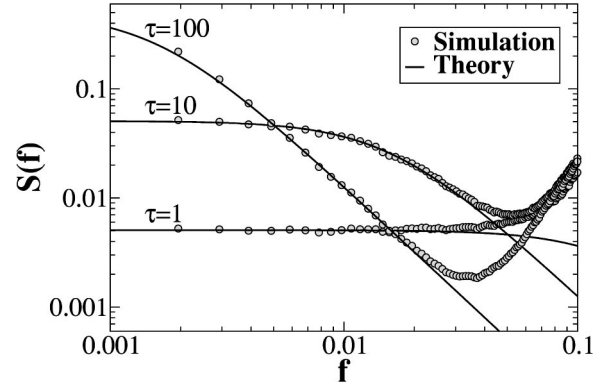


FIG. 9. The low frequency power spectrum derived from the large time Fano factor approximation Eq. (15) compared with simulation results of Eq. (1). Results for three values of the noise correlation time are shown. The variance of the noise used in the simulations is $D=0.1$. For reference, the frequency corresponding to the inverse ISI is $f=0.159$.

$$S(f) = \frac{2D\tau}{v_{th}^2} \left(\frac{1}{1 + (2\pi f\tau)^2} \right). \quad (28)$$

Just as the spike-spike autocorrelation function displays properties of the input correlation, the low frequency power spectrum of the spike train has the same Lorentzian form as the OU input. Figure 9 shows the theoretical low frequency power spectral curves for several input noise correlation times compared with simulation results.

V. CONCLUSIONS

The effects of correlated noise have been of interest in the study of many stochastic systems (see, e.g., Refs. [1,16–20]). In this study, we have seen how long-range correlated noise can influence the spike train, ISI, and spike count statistics in a perfect integrate-and-fire model. Using a quasistatic approximation, analytical expressions for the ISI density were obtained. It was seen that the exponential correlations in the noise led to exponential correlations in both the ISI sequence and the spike train at long lags. As a consequence, the power spectrum of the spike train had a Lorentzian shape at low frequencies.

An expression for the Fano factor curve was then obtained. In particular, long-range correlated noise was shown to increase the Fano factor at long time scales. Due to the finite correlation time used in the OU process, the Fano factor eventually saturates to a finite value. Such a saturation has been observed experimentally [4]. An interesting finding of our study is the fact that a minimum in spike train variability as measured by the Fano factor can be obtained in this simple model. While the perfect integrate-and-fire neuron model used here has no explicit absolute refractory period, there is a relative refractory period that arises due to the small noise and the fact that it takes a finite time (on the order of the average ISI) for the voltage to reach threshold from the reset value. It is the interaction between this refractoriness, which decreases the Fano factor for small times,

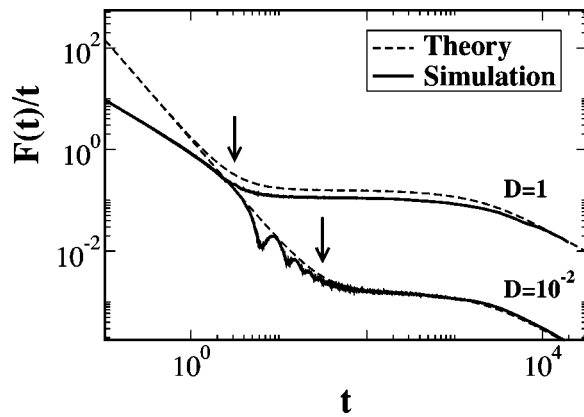


FIG. 10. The relative spike count error $F(t)/t$ as a function of counting time. The simulation results from integrating Eq. (1) are compared with the theory from the full range Fano factor approximation, $F_{\text{small}}(t) + F_{\text{large}}(t)$, where $F_{\text{large}}(t)$ is given by Eq. (15) and F_{small} is given by the envelope approximation $v_{th}/4\mu t$. Results are shown for $\tau = 1000$ and for two different values of noise, $D = 0.01$ and $D = 1$. The arrows indicate the onset of the plateau region, as given by Eq. (23). In each case the plateau persists until about the correlation time τ . While on the plateau there is very little change in the relative spike count error.

and the long-range correlated noise that will increase it for large times that causes the minimum.

It was shown that synaptic vesicle release observed in *Xenopus* neuromuscular junctions and in rat hippocampal synapses displayed long-range correlations [21]. Our slow noise could thus model the synaptic current fluctuations received by a neuron. The Fano factor minimum has been observed in the experimental data in both auditory fibers [5,6] and weakly electric fish electroreceptors [7]. Our study thus suggests that the Fano factor increase, and consequently the minimum, observed in many neurons [5,22–26] could be due to long-range correlations in the neurotransmitter secretion rate.

There is much speculation as to the significance of a minimum in spike train variability [7,8,15]. For weakly electric fish electroreceptors, the time scale at which the minimum occurred matched the observed time scale at which these fish capture prey [27], giving a behavioral relevance to this minimum. It can be shown that the discriminability d between spike counts arising from distinct signal distributions is inversely proportional to $[F(t)/t]^{1/2}$ [8,15]; this latter quantity is also the relative error of an observed spike count. Figure 10 shows the relative spike count error $F(t)/t$ as a function of counting time t for a single value of τ and two different noise intensities. The minimum of the Fano factors from Eq. (23) indicates the beginning of a plateau in the relative error. It is apparent that by increasing the counting time, while on

the plateau, there is little improvement in the accuracy of spike count estimation. However, the relative error can be reduced to arbitrarily small values by taking increasing counting times greater than the correlation time of the OU process, τ . A sensory system, using observed spike count to determine the presence or absence of prey, would encounter the problem of having to wait long periods of time for the lowest possible spike count relative error. By the time a decision is made on the presence or absence of prey, any action based on that decision would be irrelevant as the prey would have escaped in the meantime. The Fano factor might already implicitly factor in the cost of waiting too long. It is proportional to the relative error squared multiplied by counting time. The rise due to the factor of counting time implicitly accounts for the cost of indecision. If the Fano factor were actually an inverse measure of the benefit from the most accurate estimation in the shortest possible time, then its minimum would be the optimal time on which to perform computations used for signal detection, as has been observed experimentally in electric fish electroreceptors [7,27].

An accurate electroreceptor model [28] driven by long-range correlated noise and periodic forcing was shown to reproduce this observed minimum [8]. This result was later reproduced in a simpler leaky integrate-and-fire model with dynamic threshold [15] driven by both white and correlated noises without periodic forcing. In that study, negative ISI correlations, present due to a dynamic threshold [29], further decreased the Fano factor, from the value obtained with a renewal process, while the positive ISI correlations due to the slow noise increased it, giving rise to a minimum where signal detection with respect to an equivalent renewal process was greatest [15]. Here we have found that the simple generic perfect integrate-and-fire driven by long-range correlated noise is sufficient to observe the Fano minimum. In particular, the counting time at which the minimum occurred varies with noise intensity, possibly explaining the experimentally observed variability in the position of the minimum in weakly electric fish electroreceptors [7]. While the minimum arising from the perfect integrate-and-fire neuron is not as pronounced as that from the LIFDT, it is perhaps a less restrictive model. Because of this, it may be useful for the phenomenological description of the Fano factor and its minimum, and thus signal detection time scales in various sensory system experiments.

ACKNOWLEDGMENTS

The authors would like to thank Brent Doiron for his comments on and discussion about the manuscript. This work was supported by NSERC Canada and the Premier's Research Excellence Award from the government of Ontario.

[1] *Long-Range Dependent Stochastic Processes: Theory and Applications*, edited by G. Rangarajan and M. Ding (Springer, Berlin, in press).

[2] E.P. Simoncelli and B.A. Olshausen, *Annu. Rev. Neurosci.* **24**, 1193 (2001).

[3] R.F. Voss and J. Clarke, *J. Acoust. Soc. Am.* **63**, 258 (1978).

- [4] C. Koch, *Biophysics of Computation* (Oxford University Press, New York, 1999).
- [5] M.C. Teich, in *Single Neuron Computation*, edited by J. D. T. McKenna and S. F. Zornetzer (Academic, San Diego, 1992), pp. 589–622.
- [6] M.C. Teich, IEEE Trans. Biomed. Eng. **36**, 150 (1989).
- [7] R. Ratnam and M.E. Nelson, J. Neurosci. **20**, 6672 (2000).
- [8] M.J. Chacron, A. Longtin, and L. Maler, J. Neurosci. **21**, 5328 (2001).
- [9] S. Bahar, J.W. Kantelhardt, A. Neiman, H.H.A. Rego, D.F. Russell, L. Wilkens, A. Bunde, and F. Moss, Europhys. Lett. **56**, 454 (2001).
- [10] D.R. Cox and P.A.W. Lewis, *The Statistical Analysis of Series of Events* (Methun, London, 1966).
- [11] D.M. Racicot and A. Longtin, Physica D **104**, 184 (1997).
- [12] For the white noise driven case perfect integrate-and-fire, the ISI density is given by $P^{\text{WN}}(I) = v_{th} \exp[-(\mu I - v_{th})^2 / (4QI)] / \sqrt{2\pi QI^3}$, where Q is the intensity of the driving noise process. Although at first glance this resembles Eq. (9), the difference in functional form of the two expressions are distinct. This is because the power by which I enters the denominator of the exponential argument and the denominator of the entire expression is different for the two cases.
- [13] U. Fano, Phys. Rev. **72**, 26 (1947).
- [14] H. Risken, *The Fokker-Planck Equation* (Springer, Berlin, 1996).
- [15] A. Longtin, C. Laing, and M.J. Chacron, in *Long-Range Dependent Stochastic Processes: Theory and Applications*, edited by G. Rangarajan and M. Ding (Springer, Berlin, in press).
- [16] T.E. Diallynas, K. Lindenberg, and G.P. Tsironis, Phys. Rev. E **56**, 3976 (1997).
- [17] S.I. Denisov and W. Horsthemke, Phys. Rev. E **65**, 031105 (2002).
- [18] E. Salinas and T.J. Sejnowski, Neural Comput. **14**, 2111 (2002).
- [19] G. Rangarajan and M.Z. Ding, Phys. Rev. E **61**, 4991 (2000).
- [20] K. Linkenkaer-Hansen, V.V. Nikouline, J.M. Pavla, and R.J. Ilmoniemi, J. Neurosci. **21**, 1370 (2001).
- [21] S.B. Lowen, S.S. Cash, M. Poo, and M.C. Teich, J. Acoust. Soc. Am. **17**, 5666 (1997).
- [22] S.B. Lowen and M.C. Teich, J. Acoust. Soc. Am. **92**, 803 (1992).
- [23] M.C. Teich, R.G. Turcott, and R.M. Siegel, IEEE Eng. Med. Biol. Mag. **15**, 79 (1996).
- [24] S.B. Lowen and M.C. Teich, J. Acoust. Soc. Am. **99**, 3585 (1996).
- [25] R.G. Turcott and M.C. Teich, Ann. Biomed. Eng. **24**, 269 (1996).
- [26] M.C. Teich, C. Heneghan, S.B. Lowen, T. Ozaki, and E. Kaplan, J. Opt. Soc. Am. A **14**, 529 (1997).
- [27] M.E. Nelson and M.A. MacIver, J. Exp. Biol. **202**, 1195 (1999).
- [28] M.J. Chacron, A. Longtin, M. St-Hilaire, and L. Maler, Phys. Rev. Lett. **85**, 1576 (2000).
- [29] M.J. Chacron, K. Pakdaman, and A. Longtin, Neural Comput. **21**, 253 (2003).